Pulse broadening in graded-index optical fibers

Robert Olshansky and Donald B. Keck

This paper reports on some theoretical and experimental investigations of the radial refractive index gradient that maximizes the information-carrying capacity of a multimode optical waveguide. The primary difference between this work and previous studies is that the dispersive nature of core and cladding materials is taken into consideration. This leads to a new expression for the index gradient parameter α_c which characterizes the optimal profile. Using the best available refractive index data, it is found that in high-silica waveguides, the dispersive properties of the glasses significantly influence the pulse broadening of near-parabolic fibers, and that the parameter α_c must be altered by 10–20% to compensate for dispersion differences between core and cladding glasses. These predictions are supported by pulse broadening measurements of two graded-index fibers. A comparison is made between the widths and shapes of measured pulses and pulses calculated using the WKB approximation and the near-field measurement of the index profiles. The good agreement found between theory and experiment not only supports the predictions made for the value of α_c, but demonstrates an ability to predict pulse broadening in fibers having general index gradients.

I. Introduction

Communication systems of the near future will require information-carrying capacities of several hundred Mbits/sec over distances of several kilometers. Over the past few years the optical fiber waveguide has established itself as a leading contender for the transmission medium of such systems. Much effort has been expended on designing optical waveguides that will have sufficient information-carrying capacity to meet these requirements. A number of studies[1–6] have predicted that multimode fibers having a parabolic or near-parabolic radial index profile will have bandwidths 2–3 orders of magnitude greater than the bandwidth of a comparable step-index fiber. Indeed, bandwidth increases of an order of magnitude or greater have been observed[7–10] in state-of-the-art graded-index fibers.

The primary thrust of this paper is to show that factors that have heretofore been ignored can have a profound effect on the radial index profile that maximizes information-carrying capacity. It differs from the previous studies primarily in that the dispersive nature of the core and cladding glasses is taken into consideration. Using the best refractive index data available, it is found that these dispersive properties have a significant effect on the pulse broadening. The calculations indicate that the index gradient parameter α_c, which characterizes the optimal profile shape, should be altered by 10–20% to compensate for dispersion in the core and cladding glasses. These conclusions are supported by a number of measurements of pulse broadening in graded-index fibers.

To present a clearer picture, a general discussion of pulse dispersion and its characterization in the multimode optical waveguide has been included. This is found in Sec. II, which presents a general formalism for characterizing pulse broadening and identifies different mechanisms producing pulse broadening.

The WKB solution for cylindrical waveguides is discussed in Sec. III. This solution can be used to calculate pulse shapes for an arbitrary index profile. The class of index profiles introduced by Gloge and Marcatili[4] is then analyzed, and it is shown that including the effects of material dispersion leads to a significant correction to the α value that minimizes pulse broadening. Index data are presented and used to evaluate the size of this correction.

In Sec. IV, the results of measurements of two waveguides at five different wavelengths are presented and analyzed. It is shown that the pulse broadening depends strongly on the source wavelength. Calculations of the shape, width, and wavelength dependence of the pulses are presented. These show that if one accounts for differential modal excitation and attenuation and the dispersive properties of the glasses, the WKB solution gives good agreement with the observations. Hence, an interesting by-product of this work is a demonstrated capability to predict the pulse broadening in general graded-index waveguides.

The authors are with Corning Glass Works, Corning, New York 14830.

Received 15 May 1975.

II. Pulse Propagation in Graded-Index Fibers

A formalism is presented for describing the propagation characteristics of graded-index, multimode fibers. The index profiles of cylindrically symmetric waveguides can be conveniently specified by the equation

$$n^2(r) = n_1^2[1 - 2\Delta f(r/a)], \tag{1}$$

where $n(r)$ is the refractive index of the waveguide as a function of distance r from the axis, and n_1 is the index along the axis. The profile function $f(r/a)$ is defined so that it is zero on axis

$$f(0) = 0 \tag{2}$$

and becomes equal to unity at the core-cladding boundary located at $r = a$,

$$f(r/a) = 1 \quad \text{for } r \geq a. \tag{3}$$

The cladding index n_2 is thus defined to be

$$n_2 = n_1(1 - 2\Delta)^{1/2}. \tag{4}$$

The quantity Δ provides a useful measure of the core-cladding index difference. From Eq. (4) one finds

$$\Delta = (n_1^2 - n_2^2)/2n_1^2. \tag{5}$$

Each mode of the waveguide can be specified by the pair of integers μ and ν, which, respectively, specify the number of radial nodes and azimuthal nodes in the transverse electromagnetic fields of that mode. The propagation constant $\beta_{\mu,\nu}$ of each mode depends explicitly on all quantities that specify the waveguide structure and on the wavelength λ of the propagating light,

$$\beta_{\mu,\nu} = \beta_{\mu,\nu}(n_1, \Delta, a, \lambda). \tag{6}$$

The propagation constants depend on the wavelength explicitly and implicitly through the wavelength variation of n_1 and Δ. Although the index profile $f(r/a)$ may also vary slightly with wavelength, such effects will not be considered here.

For analyzing pulse transmission, one is concerned with the group delay time per unit length for the mode μ,ν. This is given by

$$\tau_{\mu,\nu} = \frac{d\beta_{\mu,\nu}}{d\omega}. \tag{7}$$

If the free space propagation constant, $k = 2\pi/\lambda$, is introduced, Eq. (7) can be rewritten as

$$\tau_{\mu,\nu} = \frac{1}{c}\frac{d\beta_{\mu,\nu}}{dk}. \tag{8}$$

If the fiber is excited by an impulse excitation and if there is no mode coupling, the impulse response, $P(t,z,\lambda)$, for spectral component λ at position z can be written as

$$P(t,z,\lambda) = \Sigma P_{\mu\nu}(\lambda,z)\delta[t - z\tau_{\mu\nu}(\lambda)], \tag{9}$$

where the summation extends over all guided modes. The distribution functions $P_{\mu\nu}(\lambda,z)$ describe the power in mode μ,ν as a function of wavelength and position. At $z = 0$ the distribution function will be determined by the spatial, angular, and spectral distribution of the source, as well as by the source-fiber coupling configuration. As the impulse propagates along the waveguide the power in each mode will change according to the attenuation occurring in that mode. It will be assumed throughout that no mode coupling occurs.

In general, only the total power integrated over all source wavelengths will be detected. Hence, the quantity of practical interest is the full impulse response

$$P(t,z) = \int_0^\infty d\lambda P(t,z,\lambda). \tag{10}$$

The propagation characteristics of the fiber can be described by specifying the moments $M_n(z)$ of the full impulse response. These moments are defined by

$$M_n(z) = \int_0^\infty dt t^n P(t,z). \tag{11}$$

In some situations, knowledge of only the first few moments is sufficient for system design considerations. If this is the case, the required amount of pulse broadening information is reduced considerably.

Equations (9)–(11) can be combined to yield

$$M_n(z) = z^n \int_0^\infty d\lambda \Sigma P_{\mu\nu}(\lambda,z)\tau_{\mu\nu}{}^n(\lambda). \tag{12}$$

The predominant wavelength dependence of the distribution function $P_{\mu\nu}(\lambda,z)$ is determined by the spectral distribution $S(\lambda)$ of the source. Even for the relatively broad LED sources, $S(\lambda)$ is a sharply peaked function whose rms width is, at most, a few percent of the mean source wavelength. One can thus define a new distribution function $p_{\mu\nu}(\lambda,z)$ by the expression

$$P_{\mu\nu}(\lambda,z) = S(\lambda)p_{\mu\nu}(\lambda,z), \tag{13}$$

where $p_{\mu\nu}(\lambda,z)$ is a slowly varying function of λ over the range where $S(\lambda)$ is nonzero.

The main wavelength dependence of the distribution function $p_{\mu\nu}$ is expected to come from such factors of the λ^{-4} dependence of the Rayleigh scattering losses or possible variations with wavelength of the spatial and angular distribution of the source. These effects are generally small and will be ignored in the remainder of the paper.

Proceeding with the analysis, it can be assumed that $S(\lambda)$ is normalized so that

$$\int_0^\infty d\lambda S(\lambda) = 1. \tag{14}$$

Consequently, the mean source wavelength λ_0 is given by

$$\lambda_0 = \int_0^\infty d\lambda \lambda S(\lambda), \tag{15}$$

and the root mean square (rms) spectral width of the source σ_s is given by

$$\sigma_s = \left[\int_0^\infty d\lambda(\lambda - \lambda_0)^2 S(\lambda)\right]^{1/2}. \tag{16}$$

The influence of the source spectral distribution on the fiber's transmission properties can be studied by expanding the delay per unit length of the μ,νth mode, $\tau_{\mu\nu}(\lambda)$, in a Taylor series about λ_0. Substituting this series into Eq. (12) and using Eq. (13) give

$$M_n(z) = z^n \int_0^\infty d\lambda S(\lambda)\Sigma p_{\mu\nu}(z) \{\tau_{\mu\nu}{}^n(\lambda_0) + n(\lambda-\lambda_0)\tau_{\mu\nu}{}^{n-1}(\lambda_0)\tau_{\mu\nu}{}'(\lambda_0) + n(\lambda-\lambda_0)^2/2\tau_{\mu\nu}{}^{n-1}(\lambda_0)\tau_{\mu\nu}{}''(\lambda_0) + n(n-1)(\lambda-\lambda_0)^2/2\tau_{\mu\nu}{}^{n-2}(\lambda_0)[\tau_{\mu\nu}{}'(\lambda_0)]^2 + \ldots\}. \quad (17)$$

Treating $p_{\mu\nu}$ as independent of λ, Eqs. (14)–(16) can be used to integrate Eq. (17) to find that

$$M_n(z) = z^n\Sigma p_{\mu\nu}(z)(\tau_{\mu\nu}{}^n(\lambda_0) + \sigma_s{}^2/(2\lambda_0{}^2) \times \{n\tau_{\mu\nu}{}^{n-1}(\lambda_0)\lambda_0{}^2\tau_{\mu\nu}{}''(\lambda_0) + n(n-1)\tau_{\mu\nu}{}^{n-2}(\lambda_0)[\lambda_0\tau_{\mu\nu}{}'(\lambda_0)]^2\}) + 0(\sigma_s{}^3/\lambda_0{}^3). \quad (18)$$

The small size of σ_s/λ_0 allows the neglect of higher order terms.

The following quantities are most useful in describing the energy distribution at z. By definition, the total power arriving at z is given by

$$M_0(z) = \Sigma p_{\mu\nu}(z); \quad (19)$$

the mean delay time of the pulse $\tau(z)$ is given by

$$\tau(z) = M_1(z)/M_0(z); \quad (20)$$

and the rms pulse width $\sigma(z)$ by

$$\sigma(z) = [M_2(z)/M_0(z) - \tau^2(z)]^{1/2}. \quad (21)$$

Combinations of higher moments further describe the power distribution, but the first three are the most important.

To simplify the notation required in the following expressions, the symbol $\langle\ \rangle$ will be used to indicate the average value of a quantity with respect to the distribution $p_{\mu\nu}$, so, for example,

$$\langle A\rangle \equiv \Sigma p_{\mu\nu}(z)A_{\mu\nu}/M_0. \quad (22)$$

From Eqs. (19)–(22), the full pulse delay time is found to be

$$\tau(z) = z[\langle\tau(\lambda_0)\rangle + \sigma_s{}^2/(2\lambda_0{}^2)\langle\lambda_0{}^2\tau''(\lambda_0)\rangle]. \quad (23)$$

For the purpose of specifying the fiber bandwidth for digital systems, Personick[11] has shown that one is primarily concerned with the rms width $\sigma(z)$. This is given by

$$\sigma(z) = (\sigma^2_{\text{INTERMODAL}} + \sigma^2_{\text{INTRAMODAL}})^{1/2} + 0(\sigma_s{}^3/\lambda_0{}^3), \quad (24)$$

where the definitions

$$\sigma^2_{\text{INTERMODAL}} = z^2\{\langle\tau^2(\lambda_0)\rangle - \langle\tau(\lambda_0)\rangle^2 + \frac{\sigma_s{}^2}{\lambda_0{}^2}[\langle\lambda_0{}^2\tau''(\lambda_0)\tau(\lambda_0)\rangle - \langle\lambda_0{}^2\tau''(\lambda_0)\rangle\langle\tau(\lambda_0)\rangle]\} \quad (25)$$

and

$$\sigma^2_{\text{INTRAMODAL}} = z^2\frac{\sigma_s{}^2}{\lambda_0{}^2}\langle[\lambda_0\tau'(\lambda_0)]^2\rangle \quad (26)$$

have been introduced.

The square of the rms width has been separated into an intermodal and an intramodal component. The intermodal term [Eq. (25)] results from delay differences among the modes and vanishes only if all delay differences vanish. This term is found to contain a dominant term and a small correction that is proportional to the square of the relative source spectral width (σ_s/λ_0). For the refractive index profiles considered in this paper, this term is found to be negligible.

The intramodal term [Eq. (26)] represents an average of the pulse broadening within each mode. It becomes the only term present in the dispersion of a single-mode waveguide. The intramodal dispersion arises from two distinct effects, a pure material effect that corresponds to the pulse broadening in bulk material and a waveguiding effect. This separation can be made explicit by writing the modal delay time in the form

$$\tau_{\mu\nu} = N_1/c + \delta\tau_{\mu\nu}, \quad (27)$$

where N_1 is material group index,

$$N_1 = n_1 - \lambda dn_1/d\lambda, \quad (28)$$

and $\delta\tau_{\mu\nu}$ represents the correction to this introduced by the waveguide structure. The derivative $\tau_{\mu\nu}{}'$ can be written as

$$\tau_{\mu\nu}{}' = -\lambda n_1{}'' + \delta\tau_{\mu\nu}{}'. \quad (29)$$

Since the intramodal contribution to the total rms pulse width is obtained by squaring and averaging over Eq. (29), one can write the intramodal contribution as

$$\sigma^2_{\text{INTRAMODAL}} = z^2\frac{\sigma_s{}^2}{\lambda_0{}^2}[(\lambda_0{}^2n_1{}'')^2 - 2\lambda_0{}^2n_1{}''\langle\lambda_0\delta\tau'\rangle + \langle(\lambda_0\delta\tau')^2\rangle]. \quad (30)$$

Hence, the total intramodal contribution has a pure material component, a waveguide component, and a mixed component arising from the cross product.

In the remainder of this paper, the primary interest will be in graded-index waveguides in which the intermodal delay differences are small. In this case, the derivative of the intermodal delay differences $\delta\tau_{\mu\nu}{}'$ is also small, and, as will be shown explicitly in the next section, the intramodal contribution is then dominated by the pure material term

$$\sigma_{\text{INTRAMODAL}} \approx \frac{\sigma_s}{\lambda_0}(\lambda_0{}^2n_1{}''). \quad (31)$$

This quantity represents the ultimate lower limit of the pulse broadening.

III. WKB Approximation

A. General Solution

The WKB approximation can be used to determine propagation constants of the cylindrically symmetric multimode waveguide having an arbitrary index profile. As shown by Gloge and Marcatili,[4] the WKB solutions are

$$(\mu + 1/2)\pi = \int_{R_1}^{R_2} dr K_{\mu\nu}(r), \tag{32}$$

where

$$K_{\mu\nu}(r) = [k^2 n^2(r) - \nu^2/r^2 - \beta_{\mu\nu}{}^2]^{1/2}, \tag{33}$$

and R_1 and R_2 are the zeros of Eq. (33). The delay time $\tau_{\mu\nu}$ can be determined by taking the derivative of Eq. (32) with respect to k, while holding μ and ν fixed. Using Eq. (1) for the index profile and taking the derivative give

$$\tau_{\mu\nu} = k/\beta_{\mu\nu}\Big[(N_1/n_1)\int_{R_1}^{R_2} dr n^2(r)/K_{\mu\nu}(r) - (\lambda\Delta'/2\Delta)\int_{R_1}^{R_2} dr[n^2(r) - n_1{}^2]/K_{\mu\nu}(r)\Big] \Big/ \int_{R_1}^{R_2} dr/K_{\mu\nu}(r). \tag{34}$$

Equation (34) is equivalent to Eq. (42) of Ref. 4 if one sets $N_1 = n_1$ and $\lambda\Delta' = 0$. Equation (34) can be used for making numerical predictions of pulse shapes once the index profile is specified. Such calculations have been carried out for two fibers whose index profiles were measured by the near field technique.[12] These calculations as well as the measured pulses will be discussed in Sec. IV.

B. Intermodal Broadening for a Class of Index Profiles

For the class of index profiles given by

$$f(r/a) = (r/a)^\alpha, \tag{35}$$

Gloge and Marcatili have derived a simple closed form approximation to the WKB solution. The propagation constant β is found to be

$$\beta_n = n_1 k\{1 - 2\Delta[n/N(\alpha)]^{\alpha/\alpha+2}\}^{1/2}, \tag{36}$$

where

$$N(\alpha) = \frac{\alpha}{\alpha + 2} a^2 k^2 n_1{}^2 \Delta. \tag{37}$$

The designation n used in Eq. (36) is not a true mode label as is the pair (μ,ν). Rather, n counts the number of modes with propagation constant β in the range

$$n_1 k \geq \beta \geq \beta_n. \tag{38}$$

The delay time for the modes can be determined from Eqs. (36)–(38) as

$$\tau_n = N_1\Big[1 + \Delta\left(\frac{\alpha - 2 - \epsilon}{\alpha + 2}\right)(n/N)^{\alpha/\alpha+2} + \frac{\Delta^2}{2}\frac{(3\alpha - 2 - 2\epsilon)}{\alpha + 2}(n/N)^{2\alpha/\alpha+2}\Big] + 0(\Delta^3), \tag{39}$$

where

$$\epsilon = \frac{-2n_1}{N_1}\frac{\lambda\Delta'}{\Delta}. \tag{40}$$

To first order in Δ the delay differences in Eq. (39) are zero if

$$\alpha = 2 + \epsilon. \tag{41}$$

Assuming that all modes propagate equal power ($p_{\mu\nu} = 1$), Eqs. (25) and (39) can be used to calculate the rms width due to intermodal broadening. If the summation required in evaluating Eq. (25) is approximated by an integration, one finds

$$\sigma_{\text{INTERMODAL}} = \frac{LN_1\Delta}{2c}\frac{\alpha}{\alpha + 1}\left(\frac{\alpha + 2}{3\alpha + 2}\right)^{1/2} \times\left[C_1{}^2 + \frac{4C_1C_2\Delta(\alpha + 1)}{2\alpha + 1} + \frac{4\Delta^2C_2{}^2(2\alpha + 2)^2}{(5\alpha + 2)(3\alpha + 2)}\right]^{1/2}, \tag{42}$$

where

$$C_1 = \frac{\alpha - 2 - \epsilon}{\alpha + 2},$$

and

$$C_2 = \frac{3\alpha - 2 - 2\epsilon}{2(\alpha + 2)}. \tag{43}$$

The minimun of the intermodal rms with width occurs for[13]

$$\alpha_c = 2 + \epsilon - \Delta\frac{(4 + \epsilon)(3 + \epsilon)}{(5 + 2\epsilon)}. \tag{44}$$

The term on the right of Eq. (44) represents a small correction to the optimal α given by Eq. (41). This correction results from a partial cancellation that occurs between the two mode dependent terms in Eq. (39) if $\alpha - 2 - \epsilon$ is of order Δ. The size of this correction changes as the distribution of power among the modes varies. Since corrections to the approximate WKB solution [Eq. (36)] can be of this same magnitude, and inaccuracies in the value of ϵ determined from measured refractive indices are also this large, Eq. (44) is adequate for the present discussion.

To enable computations to be made, it will be assumed in the remainder of this paper that $n_1(\lambda)$ and $n_2(\lambda)$ correspond to the refractive indices of TiO_2 doped fused silica and fused silica, respectively. This choice is made simply because the best available dispersion data exist for these two materials. For the index $n_2(\lambda)$ of the cladding the Sellmeier fit of Malitson[14] for fused silica has been used. For $n_1(\lambda)$ a two-term Sellmeier fit has been made to refractive index measurements made on a bulk sample of 3.4 wt % TiO_2 doped silica at eight wavelengths in the 546–1083-nm range. The estimated precision of these measurements is a few parts in 10^5.

Figure 1(A) shows the fitted values of $n_1(\lambda)$ and $n_2(\lambda)$ in the range from 0.5 μm to 1.1 μm. Figures 1(B) and 1(C), respectively, show the first and second derivatives of the refractive indices of these two glasses. Figure 2 shows the values of Δ and $\lambda\Delta'$ determined from the data. It can be observed in Fig. 2(A) that, over the range of wavelengths shown, Δ decreases by about 15%.

From the index data on Figs. 1 and 2, $\epsilon(\lambda)$ can be calculated, and a plot of α_c *vs* λ is shown in Fig. 3. The value of α_c minimizing the intermodal rms pulse width departs significantly from the optimal profile $\alpha = 2(1 - 6\Delta/5)$, which is predicted if the effect of material dispersion is ignored.

The optimal α varies quite strongly with wave-

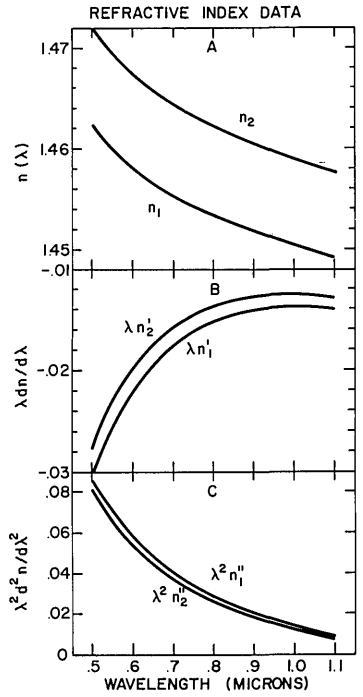

Fig. 1. Refractive index data for 3.4 wt % TiO_2 doped silica (n_1) and fused silica (n_2) are shown for (A) Sellmeier fit to the refractive index, (B) $\lambda dn/d\lambda$, (C) $\lambda^2 d^2n/d\lambda^2$.

length, decreasing from about 2.5 at 500 nm to 2.2 at 1000 nm. A waveguide with a given index profile α is thus predicted to show different pulse widths according to the source wavelength used. This wavelength-dependent pulse broadening provides a tool for observing these effects and is discussed at length in Sec. IV.

C. Intramodal Broadening for a Class of Profiles

Equation (39) for the delay time can be used to evaluate $\lambda\tau_n'$, which is required for predicting the intramodal broadening. Keeping only the largest terms gives

$$\lambda\tau_n' = -\lambda^2 n_1'' + N_1\Delta\left(\frac{\alpha - 2 - \epsilon}{\alpha + 2}\right)\left(\frac{2\alpha}{\alpha + 2}\right)\left(\frac{n}{N}\right)^{\alpha/\alpha+2}. \quad (45)$$

Since $\lambda^2 n_1''$ and Δ are the same order of magnitude, both terms contribute to $\lambda\tau_n'$ for large α (but with opposite signs). For α near α_c, the pure material term in Eq. (45) dominates. This reflects the fact that when the intermodal delay differences are small, the derivatives of these differences are also small.

Assuming equal excitation of the modes, one can perform the summation over all modes required by Eq. (26) and find that

$$\sigma_{\text{INTRAMODAL}} = \frac{\sigma_\lambda}{\lambda}\left[(-\lambda^2 n_1'')^2 - 2\lambda^2 n_1''(N_1\Delta)\left(\frac{\alpha - 2 - \epsilon}{\alpha + 2}\right)\left(\frac{2\alpha}{2\alpha + 2}\right) + (N_1\Delta)^2\left(\frac{\alpha - 2 - \epsilon}{\alpha + 2}\right)^2\frac{2\alpha}{3\alpha + 2}\right]^{1/2}. \quad (46)$$

D. Predicted Pulse Widths

The total rms pulse widths for α profiles can be predicted from Eqs. (42) and (46). In Fig. 4, this rms pulse width is shown as a function of α for three types of GaAs sources, all operating at $\lambda = 0.9$ μm, but having different spectral bandwidths. The three curves correspond to an LED, an injection laser, and a distributed-feedback laser having typical rms spectral widths of 150 Å, 10 Å, and 2 Å, respectively. The waveguide is assumed to have $n_1(\lambda)$ and $n_2(\lambda)$ of Fig. 1(A) and to propagate equal power in all modes. For comparison, a dashed curve represents the rms width predicted if material dispersion and intramodal broadening are ignored.

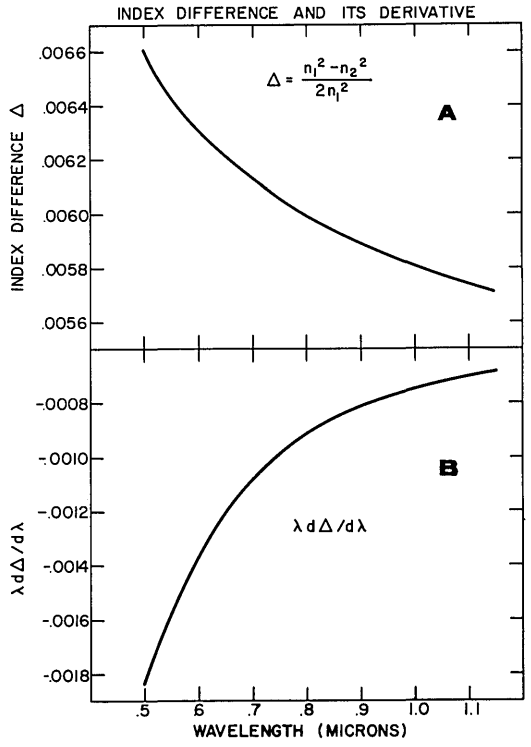

Fig. 2. The index difference Δ determined from the data of Fig. 1(A) is shown in (A), and the derivative $\lambda d\Delta/d\lambda$ is shown in (B).

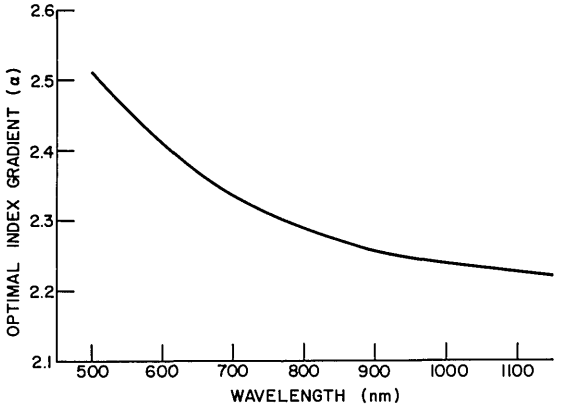

Fig. 3. The α value that minimizes the pulse broadening is shown as a function of wavelength.

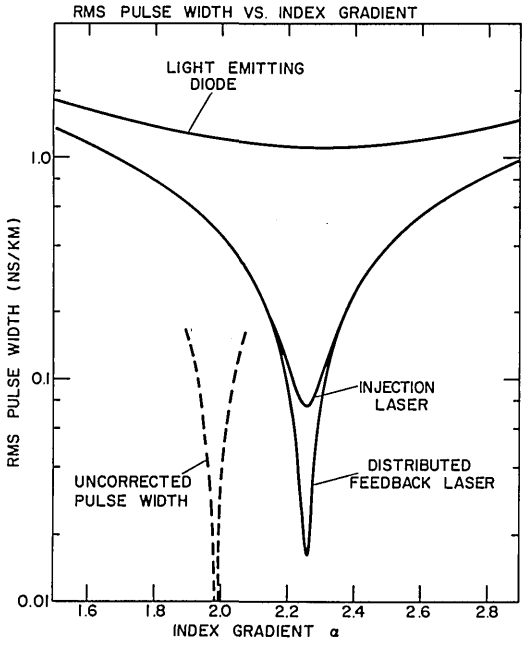

Fig. 4. Assuming equal power in all modes, the rms pulse width is shown as a function of α for three different sources, all operating at 0.9 μm. The sources are taken to be an LED, a gallium arsenide injection laser, and a distributed feedback laser having rms spectral widths of 150 Å, 10 Å, and 2 Å, respectively. The dashed curve shows the pulse width that would be predicted if all material dispersion effects were neglected.

For the LED source, pulse broadening of less than 1.5 nsec/km can be achieved if α is within 25% of the optimal value. For the injection laser, an α within 5% of the optimal will give pulse widths less than 0.2 nsec/km, and for the distributed-feedback laser, widths of 0.05 nsec/km are predicted if 1% control on α can be achieved.

IV. Wavelength-Dependent Pulse Broadening

In the previous sections it was found that the α value that minimizes the intermodal pulse dispersion departs significantly from the parabolic profile and that the magnitude of this departure depends on the wavelength of the source. In Fig. 4, one sees that the calculated rms pulse width depends very strongly on the difference between the α of the waveguide and the optimal α. As a result of these features, the rms pulse width will depend on the source wavelength for waveguides having an α value not too different from α_c. This wavelength-dependent pulse broadening is more fully analyzed in this section, and some experimental results are reported that support the analysis.

In Fig. 5, the calculated rms width is shown as a function of source wavelength for waveguides with index profiles in the range $1.5 \leq \alpha \leq 2.9$. For the purpose of illustration, it is assumed in these calculations that the rms spectral width of the source is 2 Å. For this range of α values both the intermodal and intramodal contributions must be considered.

The wavelength dependence of the intermodal term depends on the specific α value. For $\alpha < 2.2$, the intermodal pulse width decreases as λ increases, because for these α's the difference $|\alpha - \alpha_c|$ decreases with λ. The opposite occurs for $\alpha \geq 2.5$, and the intermodal pulse width increases with λ. For waveguides with $2.2 < \alpha < 2.5$, the minimal intermodal broadening occurs at one wavelength in the range 500 nm $< \lambda <$ 1100 nm. As λ is varied through this range, the intermodal broadening decreases until the optimal wavelength is reached, and thereafter it increases.

The intramodal contribution to the rms width is dominated by material dispersion. It is largest at the shorter wavelengths and decreases quite rapidly with wavelength. For a source spectral width of 2 Å, the rms width decreases from 0.1 nsec/km to 0.006 nsec/km between 500 nm and 1100 nm. The pulse width behavior shown in Fig. 5 reflects the combined effect of intermodal and intramodal pulse broadening.

A. Experimental Observations

Pulse broadening measurements were made on two 1-km long, graded-index, germania-doped silica fibers to observe this wavelength dependence and to attempt to verify the prediction made here for the optimal α value.

The experimental setup is shown schematically in Fig. 6. Pulse broadening was measured at 531 nm, 568 nm, 676 nm, and 799 nm using a mode-locked krypton laser and at 900 nm using a self-pulsing LOC gallium arsenide injection laser. The signal was detected with a germanium avalanche photodiode.

Light was injected into the test fiber through a 5-m segment of fiber in which strong mode coupling was generated by an irregular epoxy coating. The induced mode coupling loss was 7 dB. This method of input coupling insured that the same excitation con-

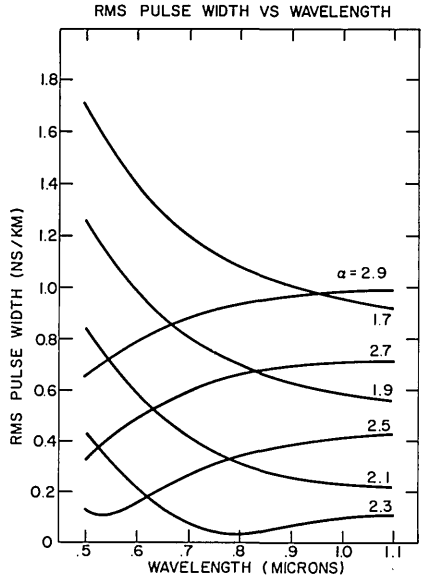

Fig. 5. For a source with 2-Å spectral width, the rms pulse width is shown as a function of wavelength for several different values of α.

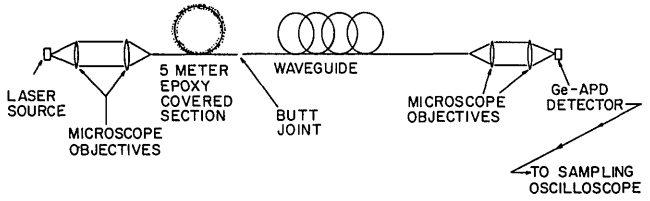

Fig. 6. A schematic representation of the pulse broadening measurement.

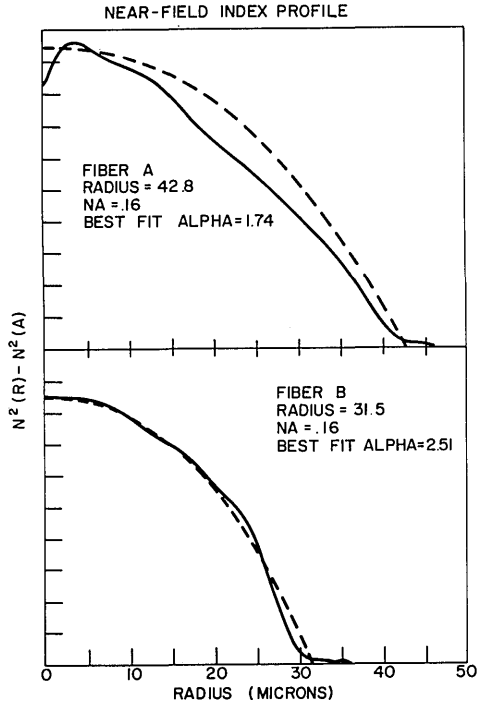

Fig. 7. The index profile $n^2(r) - n^2(a)$, determined by a near-field measurement at 900 nm, is shown for two fibers. Fiber A is best fit by $\alpha \approx 1.7$ and fiber B by $\alpha \approx 2.5$. The dashed curves show the optimal profile that passes through the end points determined from the best α fit.

ditions prevailed at all wavelengths regardless of variations in the spatial and angular distribution of the sources. Observations indicated that, without this method of input, large changes in the transmitted pulse could be obtained by off-axis illumination of the test waveguide. No such changes were observed with the mode coupled input.

Mode coupling in the test waveguide due to surface irregularities was minimized by wrapping the fibers on a special drum.[15]

The index profiles of the fibers were measured by a near-field technique,[12] and the measured profiles are shown in Figs. 7(A) and 7(B). The profile of fiber A is best fitted by $\alpha \approx 1.7$ and fiber B by $\alpha \approx 2.5$.

The output pulses observed for the two fibers at the five wavelengths are shown in Figs. 8(A) and 8(B). Fiber A exhibits about a 30% decrease in pulse width over the range of wavelengths measured, in good agreement with the prediction shown in Fig. 5 for $\alpha = 1.7$. An increase of about 20% over the range of measured wavelengths was expected for the fiber with $\alpha = 2.5$. Only a slight change in pulse width was actually observed, however, and it was in opposition to this expected increase.

B. Analysis

An understanding of these measurements requires a more detailed theoretical treatment of pulse broadening. The predictions of Fig. 5 are for waveguides having an exact α-type profile. The measured profiles show considerable variation from the fitted α profiles. The effect of these variations on the modal delays can be calculated by using the WKB solution [Eq. (34)]. Such a calculation has been carried out by making a fifteen-term polynomial fit to the near-field data and then numerically calculating the delay time for each mode.

Theoretical output pulses were generated by assuming that the response of each mode was a Gaussian pulse and summing over all modes using an appropriate power distribution function. For the rms width of the Gaussian pulse, 0.4 nsec was chosen as a reasonable estimate of the combined effects of the temporal width of the source, the response time of the detector, and the intramodal pulse broadening. The distribution function $p_{\mu,\nu}$ was chosen to reflect the steady-state modal distribution of the epoxied section used for input coupling and to reflect the strong attenuation of the higher-order modes typically observed in optical fibers.[16] From the calculated steady-state distributions in graded-index fibers with random bends,[17] it is found that the simplified form

$$p_{\mu\nu} = 1 - (m/M_c) \quad m \leq M_c,$$
$$p_{\mu\nu} = 0 \quad m > M_c, \tag{47}$$

gives a good approximation to the steady-state distribution for graded-index fibers with $1.5 < \alpha < 3.0$. In Eq. (47), m is the principal mode number defined by

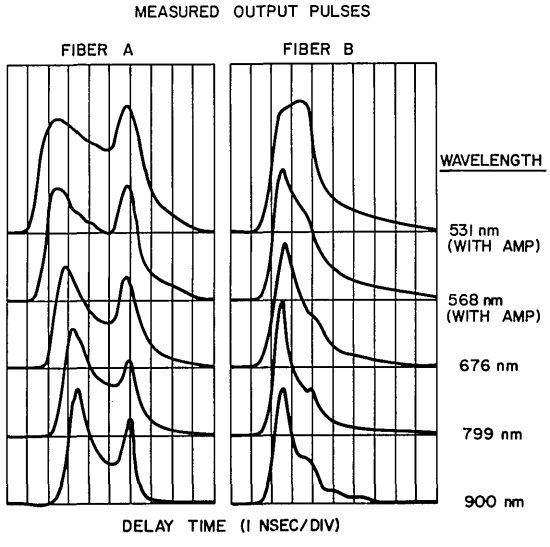

Fig. 8. Output pulses measured at five wavelengths are shown for fibers A and B.

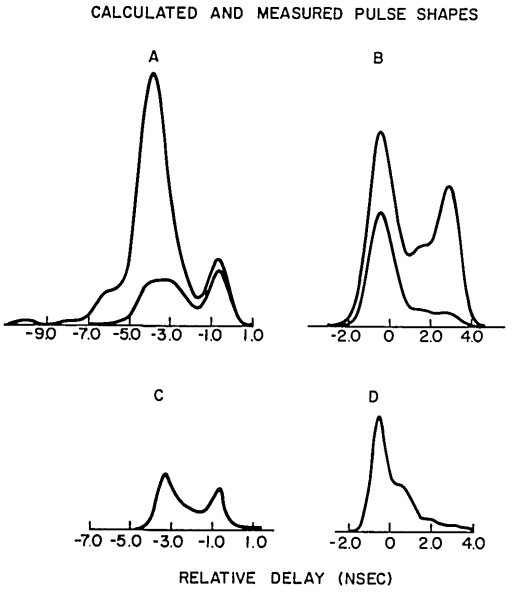

Fig. 9. Two calculated pulses for each fiber are shown in (A) and (B), and the corresponding measured pulses are shown below in (C) and (D). The larger of the two calculated pulses corresponds to equal power in all modes and the smaller pulse to the power distribution given by Eqs. (47)–(49).

$$m = 2\mu + \nu, \tag{48}$$

and M_c represents the maximum value of m that propagates over 1 km. From studies of a fiber's effective numerical aperture as a function of length,[16,18] it is found that after 1 km,

$$M_c \approx 0.9 M_{\mathrm{MAX}}, \tag{49}$$

where M_{MAX} is the theoretical maximum value of m that can occur for the guided modes.

Figures 9(A) and 9(B) each shows two calculated pulses for fibers A and B at 0.9 μm, and Figs. 9(C) and 9(D) show the corresponding measured pulses. For each fiber, the larger of the two calculated pulses corresponds to equal excitation of all modes, and the smaller pulse is calculated using Eqs. (47)–(49) for the power distribution. It is seen that the form used for the output power distribution greatly improves the agreement between the predicted and measured pulse shapes. If all modes are equally excited, the theoretical pulse shape for either fiber has two peaks. In fiber A, the earlier arriving peak is composed of higher-order modes and the later arriving peak of lower-order modes. The opposite holds true for fiber B. This can qualitatively be predicted from the best fit α and Eq. (39). As a result of the reduced power in the higher-order modes implicit in Eq. (47), the peak composed of the higher-order modes is greatly reduced in the pulses calculated using Eqs. (47)–(49). Although other forms for the output power distribution can improve the agreement between the predicted and measured pulse shapes, Eq. (47) has been used since it is a more justifiable choice for the power distribution based on present understanding of the factors involved.

Figures 10(A) and 10(B) show the predicted pulses at λ = 0.5 μm, 0.7 μm, and 0.9 μm. The horizontal scale is in nanoseconds, and the delay time is measured relative to the arrival time of the lowest-order mode. A strong wavelength dependence of the pulse width is calculated for fiber A, and only very slight dependence is calculated for fiber B. This is in agreement with the observations.

Examination of the calculated modal delay times reveals the explanation for the absence of appreciable

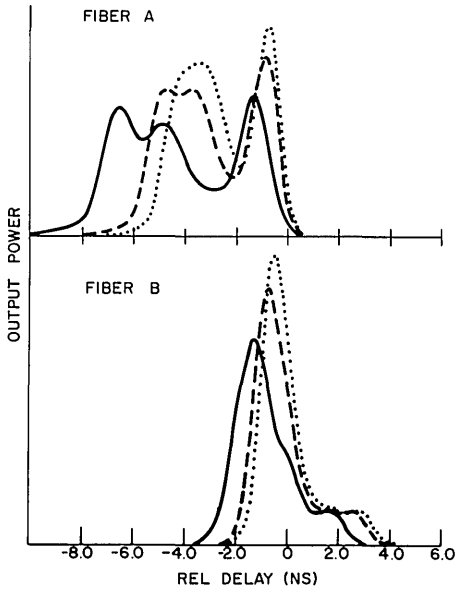

Fig. 10. Calculated pulses for fibers A and B are shown at three wavelengths. The pulses are shown for 500 nm (solid lines), 700 nm (dashed lines), and 900 nm (dotted lines). Zero relative delay corresponds to the arrival of the lowest order mode.

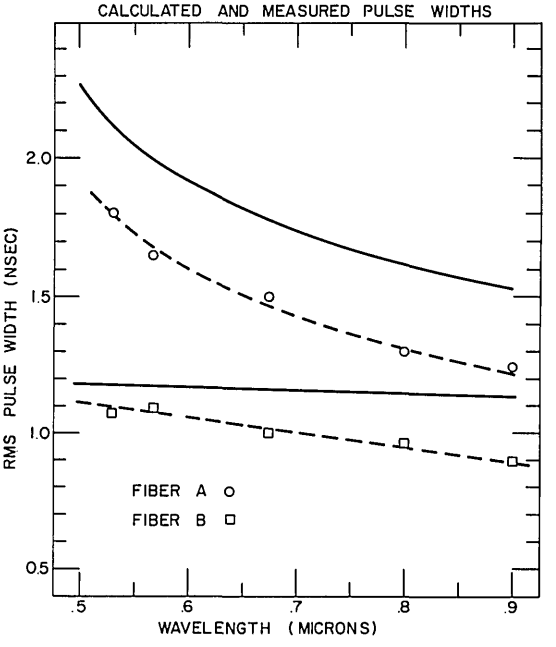

Fig. 11. Calculated rms pulse widths (solid lines) and the rms width determined from experiment (dashed lines) are shown.

wavelength dependence in waveguide B. Because the index profile varies about the optimal profile [Fig. 7(B)], the modes divide into two groups according to whether they are faster or slower than the lowest-order mode. Because of the wavelength dependence of the delay times, contained in Eq. (34), it is found that as the wavelength is increased, the faster modes arrive more nearly at the arrival time, $\tau = 0$, of the lowest-order mode. For the slower modes the relative arrival time increases. Therefore, as the wavelength is increased, the pulse tends to shift to a later arrival time, rather than to narrow. In fiber A all modes belong to the group of faster modes as is qualitatively expected for $\alpha = 1.7$. Consequently, as λ increases, all delay differences decrease, and the total pulse narrows.

Finally, in Fig. 11, the rms widths determined from the measured pulses are compared to the calculated rms widths based on the WKB theory and power distribution of Eq. (47). The slopes of the two curves are in excellent agreement. The calculated pulses lie about 20% higher than the measured pulses. The cause of this discrepancy is not known, although an effect of this size could easily be caused by a small amount of mode coupling.

V. Conclusions

Pulse broadening in two germania-doped, graded-index, multimode waveguides has been measured at five wavelengths. The measured pulse widths were found to vary strongly with wavelength in one fiber, but not in the other. A theoretical analysis based on the WKB method and near-field index profile was able to account for the observed wavelength dependence in both fibers.

On the basis of these results, the following conclusions can be drawn. First, the observed wavelength dependence is a result of the differing dispersive properties of core and cladding glasses. In order to achieve maximum information carrying capacity, the radial index profile must be modified to compensate for this. The good agreement found between the observed and calculated pulse broadening indicates that titania and germania-doped silica waveguides have nearly the same wavelength dependent dispersion. Therefore, an α about 15% greater than 2 is required for optimal compensation for sources operating near 900 nm. Second, a WKB calculation that includes the effect of dispersive properties of core and cladding glasses and the modal power distribution gives good predictions of the output pulse shape as well as the wavelength dependence of the rms width. Since the small systematic discrepancy between the calculated and measured rms pulse widths may be caused by the presence of a small amount of mode coupling, there is no reason at present to attribute this discrepancy to inaccuracies in the theoretical analysis.

References

1. S. E. Miller, Bell Syst. Tech. J. **44,** 2017 (1965).
2. S. Kawakami and J. Nishizawa, IEEE Trans. Microwave Theory Tech. **MIT-16,** 814 (1968).
3. T. Ochida, M. Furukawa, J. Kitano, K. Koizumi, and H. Matsumura, IEEE J. Quantum Electron. **QE-6,** 606 (1970).
4. D. Gloge and E. A. J. Marcatili, Bell Syst. Tech. J. **52,** 1563 (1973).
5. M. Ikeda, IEEE J. Quantum Electron. **QE-10,** 362 (1974).
6. C. C. Timmermann, AEU **28,** 344 (1974).
7. R. Bouille and J. R. Andrews, Electron. Lett. **8,** 309 (1972).
8. D. Gloge, E. L. Chinnock, and K. Koizumi, Electron. Lett. **8,** 562 (1972).
9. D. B. Keck and R. D. Maurer, in (to be published) *Proc. Microwave Research Institute Int. Symp.* (1975), Vol. 13.
10. L. G. Cohen, P. Kaiser, J. B. MacChesney, P. B. O'Connor, and H. M. Presby, in *Technical Digest of OSA Topical Meeting on Optical Fiber Transmission* (Optical Society of America, Wash. D.C., 1975).
11. S. D. Personick, Bell Syst. Tech. J. **52,** 843 (1973).
12. M. C. Hudson, D. B. Keck, and R. Olshansky (investigation of the near-field technique is currently in progress and will be reported).
13. R. Olshansky and D. B. Keck, in *Technical Digest of OSA Topical Meeting an Optical Fiber Transmission* (Optical Society of America, Wash. D.C., 1975).
14. I. M. Malitson, J. Opt. Soc. Am. **55,** 1205 (1965).
15. D. B. Keck, Proc. IEEE **62,** 649 (1974).
16. D. B. Keck, Appl. Opt. **13,** 1882 (1974).
17. R. Olshansky, Appl. Opt. **14,** 935 (1975).
18. M. C. Hudson, Corning Glass Works; private communication.

A function from feeling inferior
Felt life monotonically drearier
With a hell of a yell
It jumped into L
And converged to the limit superior.

Leo Moser. This is one of the verses found in the papers of the late Leo H. Moser; it is printed here by permission of William Moser of McGill University.